Organic & Biomolecular Chemistry

COMMUNICATION

View Article Online
View Journal | View Issue

Cite this: *Org. Biomol. Chem.*, 2014, **12**, 7932

Received 2nd July 2014,
Accepted 28th August 2014

DOI: 10.1039/c4ob01373e

www.rsc.org/obc

Estimating the shape and size of supramolecular assemblies by variable temperature diffusion ordered spectroscopy†

Benjamin M. Schulze, Davita L. Watkins, Jing Zhang, Ion Ghiviriga and Ronald K. Castellano*

Reported is characterization of the self-assembly of π-conjugated oligomers, molecules studied recently in photovoltaic devices, using variable temperature diffusion ordered spectroscopy (VT-DOSY). Iterative fitting of diffusion coefficient *versus* temperature data to a modified Stokes–Einstein equation, molecular modelling, and comparison to non-assembling model compounds, has allowed estimation of assembly size, shape, and molecularity.

Diffusion ordered spectroscopy (DOSY) is a diffusion nuclear magnetic resonance (NMR) technique that is useful for aggregate molecularity, size, and shape determination.[1] In a number of cases, DOSY NMR has been used to rigorously characterize synthetic supramolecular assemblies.[1d,f,2] Although not often coupled with variable temperature (VT) NMR, the combined techniques report on dynamic assembly processes in solution.[2d,f] Reported here is an approach using VT-DOSY to understand the self-assembly of organic π-conjugated oligomers, molecules studied recently in thin film photovoltaic devices, mutually by π-stacking and hydrogen bonding.[3] We believe that this characterization method is underutilized in a community where drawing relationships between molecular/supramolecular structure and ultimately device function is challenging but central to rational materials design.

We recently demonstrated how the photovoltaic power conversion efficiency of a branched oligothiophene (**BQPH**; Fig. 1): fullerene blend was enhanced (twofold) through hydrogen bond promoted self-assembly relative to control devices fabricated from chromophores incapable of hydrogen bonding (*e.g.*, **BQPME**).[3] Elegant previous work of Lehn and Zimmerman inspired the molecular design that features the phthalhydrazide (**PH**) heterocycle, a building block shown to form robust hydrogen-bonded assemblies in solution and on surfaces, including cyclic trimers (*i.e.*, $(\mathbf{PH})_3$).[4] In the context of

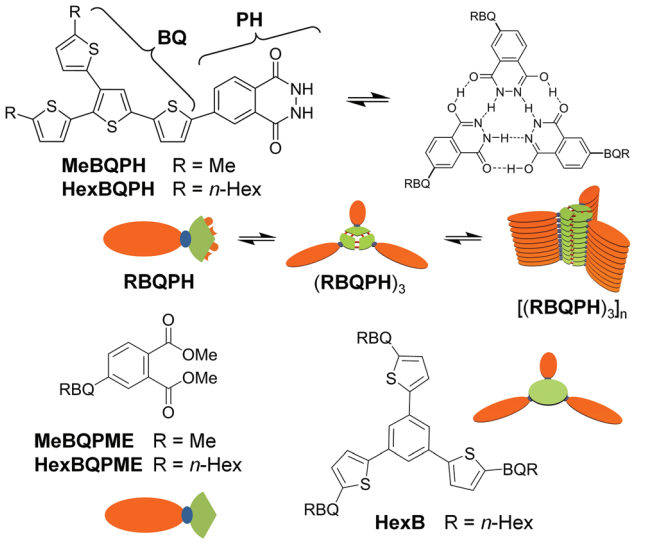

Fig. 1 Chemical and schematic representations of **HexBQPH**, **HexBQPME**, and **HexB**. Also shown is the self-association of **HexBQPH** into trimeric discs *via* hydrogen bonding followed by the formation of columnar stacks through π–π interactions.

BQPH, we suspected that its putative H-bonded rosettes (*i.e.*, $(\mathbf{BQPH})_3$) might further organize into π-stacked columnar nanostructures (*i.e.*, $[(\mathbf{BQPH})_3]_n$), an appealing chromophore arrangement (if extendable to thin films) for bulk heterojunction photovoltaics. Indeed, columnar arrangements of $(\mathbf{PH})_3$-based assemblies have been characterized before.[4a] Herein, we provide supporting evidence of this mechanism of assembly in solution for **HexBQPH** by VT-DOSY NMR by employing a modified Stokes–Einstein equation that allows derivation of molecular size in solution for objects with non-spherical shape.[1e] Facilitating the analyses is comparison of the solution behavior of **HexBQPH** to two molecules incapable of H-bonded assembly, **HexBQPME** (a model of the monomer)[3] and **HexB**[5] (a covalent analogue of the H-bonded trimer).

A ^{1}H NMR spectrum of **HexBQPH**[3] (10 mM) in the hydrogen bond promoting solvent toluene-d_8 (see Fig. S1†) shows two

Department of Chemistry, University of Florida, P.O. Box 117200, Gainesville, Florida, USA. E-mail: castellano@chem.ufl.edu

†Electronic supplementary information (ESI) available: Full experimental procedures and characterization data. See DOI: 10.1039/c4ob01373e

broadened peaks at δ = 12.78 and 13.75 ppm at 27 °C. The signals are consistent with the –NH and –OH protons of **HexBQPH**, respectively, in its lactim–lactam tautomeric form. That the peaks are well-separated and shifted far downfield suggest both H-bonded assembly and slow monomer–aggregate exchange on the NMR time scale.[4a] Also observed by ^{1}H NMR are significantly broadened and upfield shifted (up to 0.5 ppm) thiophene –CH resonances, indicative of π-stacking. In contrast, **HexBQPME** displays sharp peaks in the ^{1}H NMR spectrum under the same conditions (not shown). Upon warming through 90 °C, the –NH/–OH peaks of **HexBQPH** coalesce at ~ 85 °C (but remain significantly deshielded) and the aromatic signals sharpen (completely at ~75 °C) and shift downfield. The results are consistent with a transition from π-stacked, H-bonded assemblies to discrete H-bonded assemblies in solution.[3]

Prior to VT-DOSY studies, an analogous 1-D VT ^{1}H NMR study was performed with comparator **HexB** (see Fig. S2†). The design of this compound was suggested by computational modelling of the anticipated trimeric assembly of **HexBQPH**, that gave its approximate molecular dimensions (see Fig. S3–S5†). Preparation of phenyl cored thiophene dendrimer[5] **HexB** came *via* three-fold Suzuki coupling of the boronic ester of **HexBQ**[3] with 1,3,5-tris(5-bromothiophen-2-yl)benzene (see Scheme S1†).[6] Compared to **HexBQPH** under identical conditions, the ^{1}H NMR spectrum of **HexB** shows some broadening and upfield shifting (up to ~0.15 ppm) of the thiophene protons (in the 6.9–7.3 ppm region) and benzene core protons (at 7.1 ppm) at room temperature; again the aromatic proton peaks sharpen and move on average downfield upon raising the temperature. While the result may speak to some aggregation through π-stacking, the less pronounced chemical shift changes suggest weaker π–π association for **HexB** *versus* **HexBQPH** (*vide infra*).

Obtained from DOSY NMR experiments are translational diffusion coefficients (D) which are related to molecular size through the well-known Stokes–Einstein equation:

$$D = \frac{k_B T}{6\pi\eta r_h} \tag{1}$$

where k_B is the Boltzmann constant, T is the temperature, r_h is the hydrodynamic radius, and η is the viscosity of the solvent.[1e,7] Eqn (1) assumes that the diffusing entity is a sphere (Fig. 2a) and is large relative to the van der Waals volume of the solvent.[1e] Given these assumptions, the equation does not necessarily best describe the diffusion of the molecular entities considered here, including the self-assembled aggregates of **HexBQPH**. Therefore, the equation has been augmented as discussed by Macchioni and coworkers[1e] to include shape- and size correction factors. In modified form (eqn (2)):

$$D = \frac{k_B T}{c f_s \pi\eta r_h} \tag{2}$$

$$c = \frac{6}{1 + 0.695\left(\frac{r_{vdW}}{r_h}\right)^{2.234}} \tag{3}$$

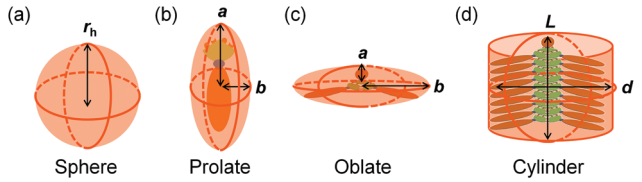

Fig. 2 Shapes of diffusing entities modelled as a (a) sphere, as in the Stokes–Einstein equation, or a (b) prolate spheroid, (c) oblate spheroid, and (d) cylinder as accommodated by a modified Stokes–Einstein equation. Represented within shapes (b)–(d) is **RBQPH** and its assemblies.

$$f_s = \frac{\left[\sqrt{1-\left(\frac{b}{a}\right)}\right]^2}{\left(\frac{b}{a}\right)^{\frac{2}{3}} \ln\left[\frac{1+\left(\sqrt{1-\left(\frac{b}{a}\right)}\right)^2}{\frac{b}{a}}\right]} \tag{4}$$

$$f_s = \frac{\sqrt{\left(\frac{b}{a}\right)^2 - 1}}{\left(\frac{b}{a}\right)^{\frac{2}{3}} \tan^{-1}\sqrt{\left(\frac{b}{a}\right)^2 - 1}} \tag{5}$$

where c is a size correlation factor between r_h of the diffusing species and the van der Waals radius (r_{vdW}) of the solvent[1e,8] (eqn (3)), and f_s is a system-derived shape friction correction factor (eqn (4) and (5)).[1e,9] The diffusing entities represented by f_s are mathematically modelled as prolate (cigar-shaped; eqn (4) and Fig. 2b) or oblate (pancake-shaped; eqn (5) and Fig. 2c) spheroids and are parameterized by the axial (a) and equatorial (b) axes of the respective spheroids (Fig. 2).[1e,9] Alternatively, f_s can be modelled as a cylinder (Fig. 2d) parameterized by the length (L) and diameter (d) (see the ESI† for details).[10] An important consequence of using eqn (2) and (3) is that r_h now represents the hydrodynamic radius of a sphere with equivalent volume to that of the spheroid used to calculate f_s.[1e]

Given eqn (2), for a monomeric species a plot of the diffusion coefficient D *versus* (T/η) should result in a straight line with a slope inversely related to c, f_s, and r_h. One can then use an iterative fitting procedure to estimate physical parameters a and b (or L and d) from the data, given a priori knowledge and shape/size constraints offered by molecular modelling (see Fig. S3–S5†). The latter provides critical guidance and can afford, for example, initial values for a and/or b (L and/or d), an approximation of the molecule's aspect ratio (*i.e.*, $2a/2b$), and a starting ellipsoid shape model (Fig. 2) for the fitting. The interdependence of several parameters (*e.g.*, c is derived from r_h; f_s is derived from b/a) means that only a, b, and r_h need to be iteratively varied. Combinations are sought that arrive at a derived (fitted) slope that matches the experimental one (typically within 0.2%). Then, the values of a and b

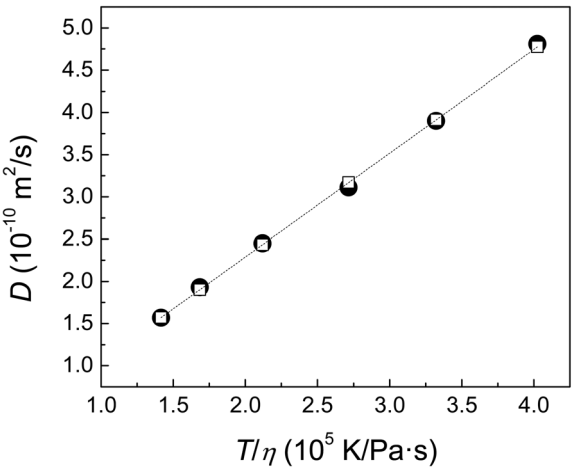

Fig. 3 Linearized [●] variable temperature diffusion data for **HexBQPME** (24 mM; DMSO-d_6). The linear regression fit is shown for data derived from the prolate [□] spheroid model and iteratively determined values of *a*, *b*, and r_h.

can be proportionally varied such that the calculated volume of the spheroid matches (typically within 1%) a spherical value derived from r_h. Worth noting, since the ratio of *a* to *b* directly determines f_s, proportional changes to both do not affect this parameter. Also clear from the treatment is that the diffusion behavior fitted *via* one model cannot be fitted using another model and that when selected, the prolate model will result in $f_s < 1$, whereas the oblate model will result in $f_s > 1$. Worth noting is that compensatory effects involving *c* and f_s can give rise to a cf_s product ~ 6 and apparent agreement with the classical Stokes–Einstein equation.[1e]

The approach is illustrated in Fig. 3 through an evaluation of **HexBQPME** in DMSO-d_6. Worth noting, temperature gradients within our samples were minimized by the use of a well designed heating and cooling system, and a convection correction was implemented within pulse sequencing to ensure accurate measurements of diffusion coefficients.[11] Diffusion constants were recorded and plotted against (T/η) (Fig. 3, dark circles); a linear fit provides the slope (*i.e.*, 1.23×10^{-15} m^3 kg^{-1}) which is inversely related to *c*, f_s, and r_h. An initial estimate of *a* (13 Å) is entered based on molecular modelling (see the ESI† for calculations), and an iterative fitting to determine a reasonable combination of *a*, *b*, and r_h ensues. In one fit (open squares), the prolate model yields values of *a* = 13 Å, *b* = 7.4 Å, and r_h = 9.0 Å, ultimately resulting in f_s = 0.69 and *c* = 5.8 (Table 1). Use of the oblate model for **HexBQPME** (which changes the value of f_s) does not fit the experimental data (data not shown).

Two solvent types were selected for variable temperature DOSY studies of **HexBQPH**. Results from toluene-d_8, an assembly promoting solvent, can be evaluated against the VT-NMR data discussed above. Studies in assembly suppressive (*i.e.*, H-bond competitive) solvents, such as dimethyl sulfoxide-d_6 (DMSO-d_6), allow direct comparison with the monomeric controls, **HexBQPME** and **HexB**. Diffusion coefficients were first collected for **HexBQPH** in DMSO-d_6. Satisfyingly, fits of the diffusion coefficient *versus* temperature data using the prolate spheroid parameters provides good agreement (Table 1) with **HexBQPME**, expected given the similar molecular dimensions of the two based on modelling (see Fig. S3–S5†). The slightly larger apparent size of **HexBQPH** might be explained through its strong hydrogen bonding with the solvent. Similar evaluation of **HexB** (in THF-d_8 due to solubility) using the oblate parameters provides values of *a* and *b* consistent with its molecular dimensions derived from modelling and an unaggregated species.

Next, variable temperature diffusion data was collected in toluene-d_8 for **HexBQPME**, **HexBQPH**, and **HexB**. Evidence for the aggregation of **HexBQPH** is immediately provided through its small diffusion coefficient ($1.03 \pm 0.01 \times 10^{-10}$ m^2 s^{-1}) relative to **HexBQPME** ($5.90 \pm 0.06 \times 10^{-10}$ m^2 s^{-1}) at 22 °C. Linearization of the diffusion *versus* temperature data and iterative fitting was first performed on **HexBQPME**. Using the prolate spheroid model, values of *a* = 14 Å, *b* = 7.8 Å, and r_h = 9.5 Å could be derived (Table 2), values which are similar to **HexBQPH** and **HexBQPME** in DMSO-d_6 (Table 1). The data is consistent with the conclusion that **HexBQPME** is monomeric in both DMSO-d_6 and toluene-d_8, and that **HexBQPH** is monomeric in DMSO-d_6.

Upon linearization of the diffusion coefficient data for **HexBQPH** (Fig. 4), bimodal behaviour is found reflected by the distinct slope change observed at approximately 60 °C. The temperature, based on 1-D VT ^{1}H NMR data (*vide supra*), is consistent with a transition from π-stacked aggregates to discrete H-bonded aggregates.[12] That the dynamic assembly process likely involves conversion of columnar π-stacks of trimers (*i.e.*, [(**HexBQPH**)$_3$]$_n$) to non-π-stacked trimeric assemblies (*i.e.*, (**HexBQPH**)$_3$) comes through iterative fitting of the two temperature ranges (21.8–52.6 °C and 58.8–92.2 °C) and

Table 1 Size and shape parameters for **HexBQPH**, **HexBQPME**, and **HexB** monomers based on VT-DOSY data

Molecule	Model[c]	*a* (Å)[d] [a_{calcd}][e]	*b* (Å)[d] [b_{calcd}][e]	*p*[f]	r_h [d] (Å)	f_s	*c*
HexBQPME[a]	P	13 [13]	7.4	1.8	9.0	0.69	5.8
HexBQPH[a]	P	15 [12]	8.1	1.9	10	0.71	5.8
HexB[b]	O	4.7	32 [24]	6.9	17	1.3	5.9

[a] Based on diffusion coefficients measured in DMSO-d_6 (**HexBQPH** = 27 mM; **HexBQPME** = 24 mM). [b] Based on diffusion coefficients measured in THF-d_8 (**HexB** = 30 mM). [c] O = oblate; P = prolate. [d] Estimated fitting error: ± 10% for *a*, *b*, and r_h. [e] Calculated parameters are estimated from molecular modelling (see the ESI for details). [f] *p* = (semimajor axis)/(semiminor axis).

Table 2 Size and shape parameters for **HexBQPH**, **HexBQPME**, and **HexB** in toluene-d_8 based on VT-DOSY data[a]

Molecule	Model[d]	a [e] (Å)	b [e] (Å)	L [e] (Å)	d [e] (Å)	r_h [e] (Å)	f_s	c
HexBQPME	P	14	7.8	—	—	9.5	0.69	5.7
HexBQPH[b]	O	26	28	—	—	27	1.0	6.0
HexBQPH[b]	C	—	—	38	51	27	1.0	6.0
HexBQPH[c]	O	5.0	26	—	—	15	1.2	5.9
HexBQPH[c]	C	—	—	7.0	51	15	1.2	5.9
HexB	O	4.5	30	—	—	16	1.3	5.9
HexB	C	—	—	7.8	58	17	1.2	5.9

[a] Based on diffusion coefficients determined at the following concentrations: **HexBQPH** = 20 mM; **HexBQPME** = 20 mM; **HexB** = 18 mM. [b] Based on data acquired at low temperature (21.8–52.6 °C). [c] Based on data acquired at higher temperature (58.8–92.2 °C). [d] C = cylinder; O = oblate; P = prolate. [e] Estimated fitting error: ± 10% for a, b, L, d, and r_h.

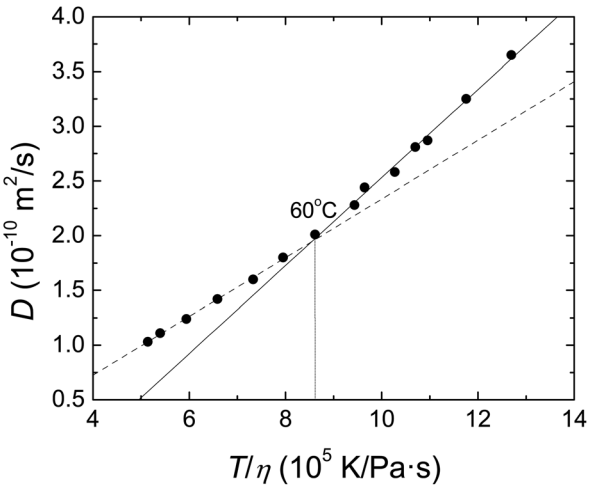

Fig. 4 Linearized variable temperature diffusion data for **HexBQPH** (20 mM; toluene-d_8). The slope change at ~ 60 °C is evident from the intersection of the solid and dashed linear regression fits.

comparison to **HexB**. Using first the oblate model for parameterization, the low temperature regime returns a = 26 Å and b = 28 Å (r_h = 27 Å) while the high temperature regime provides a = 5.0 Å and b = 26 Å (r_h = 15 Å). The equatorial radius (b) is very similar across both ranges and further similar to the calculated end-to-end length of **HexBQPH** (25 Å; see ESI† for details). Shown is that upon increasing the temperature, **HexBQPH** experiences a significant size change *only* in one dimension (from a = 26 Å to a = 5.0 Å); this is consistent with columnar growth. Confirmation that the high temperature assembly is highly represented by a discrete trimer comes through comparison with **HexB**. A plot of D *versus* (T/η) for **HexB** in toluene-d_8 gives a linear fit, suggesting that there is little extended aggregation of this species under these conditions (*vide supra*). Iterative parameter fitting using the oblate spheroid model provides a = 4.5 Å, b = 30 Å, and r_h = 16 Å. These values indeed match well with both the modelled **HexB** structure (see Fig. S5†) and the high temperature values for **HexBQPH**.

To verify our analysis, the diffusion data for **HexBQPH** and **HexB** in toluene-d_8 were alternatively subjected to iterative fitting using a cylindrical model (*i.e.*, treatment of the diffusing entity as a cylinder). Consistent results are obtained (Table 2), where for **HexBQPH** only a change in the length (L) of the cylindrical aggregates is observed as a function of temperature (21.8–52.6 °C: L = 38 Å, 58.8–92.2 °C: L = 7 Å), while the diameter (d) remains roughly the same. The **HexB** cylindrical parameters (L = 7.8 Å; D = 58 Å) are both consistent with those derived from the **HexB** oblate fitting and for **HexBQPH** at higher temperatures.

The molecularity of the **HexBQPH** aggregates can be estimated by appropriately scaling the volumes derived from the r_h values.[1e] Monomeric **HexBQPH** and **HexBQPME** have r_h ~ 9.5 Å (and equivalent sphere volume of ~ 3600 Å^3) and are assigned a molecularity of 1. Both spheroid fitting routines of **HexBQPH** in toluene-d_8 (r_h = 27 Å) yield an average molecularity of 23 on the basis of equivalent sphere volume for the low temperature regime, which corresponds to an average supramolecular assembly of ~ 6 trimeric discs. The r_h value of 15 Å (from both fitting routines) for the high temperature regime equates to an average molecularity of 3.9. This value, when coupled with the shape parameters a and b (or L and d) and molecular modelling results, strongly supports the presence of a discotic trimeric aggregate.

Conclusions

In conclusion, an iterative method for size and shape approximation involving variable temperature diffusion measurements has been exploited for the characterization of organic π-conjugated chromophore assembly in solution. Diffusion coefficients were collected *via* DOSY NMR, linearized, and fitted to a modified Stokes–Einstein equation using prolate spheroid, oblate spheroid, and cylindrical models. **HexBQPH** self-assembly showed a bimodal temperature response in toluene-d_8, consistent with a transition from columnar assemblies to isolated H-bonded trimers based on comparisons with non-assembling model compounds. We are hopeful that this approach can serve as a complementary way to explore dynamic supramolecular assembly in solution and facilitate drawing relationships between structure and function in application-oriented organic systems.

Acknowledgements

We are grateful for grant support from the National Science Foundation (CHE-1057411) and the Research Corporation for Science Advancement (Scialog Award 20316). B.M.S. acknowledges the U.S. Air Force for financial support. We also thank Prof. Jiangeng Xue for insightful discussions.

Notes and references

1 (*a*) K. F. Morris and C. S. Johnson, *J. Am. Chem. Soc.*, 1992, **114**, 3139–3141; (*b*) O. Mayzel and Y. Cohen, *J. Chem. Soc., Chem. Commun.*, 1994, 1901–1902; (*c*) M. Pons and O. Millet, *Prog. Nucl. Magn. Reson. Spectrosc.*, 2001, **38**, 267–324; (*d*) Y. Cohen, L. Avram and L. Frish, *Angew. Chem., Int. Ed.*, 2005, **44**, 520–554; (*e*) A. Macchioni, G. Ciancaleoni, C. Zuccaccia and D. Zuccaccia, *Chem. Soc. Rev.*, 2008, **37**, 479–489; (*f*) S. V. Kharlamov and K. L. Shamil, *Russ. Chem. Rev. (Engl. Transl.)*, 2010, **79**, 635–653.

2 (*a*) R. Dobrawa, M. Lysetska, P. Ballester, M. Grüne and F. Würthner, *Macromolecules*, 2005, **38**, 1315–1325; (*b*) L. Allouche, A. Marquis and J.-M. Lehn, *Chem. – Eur. J.*, 2006, **12**, 7520–7525; (*c*) Z. Chen, V. Stepanenko, V. Dehm, P. Prins, L. D. A. Siebbeles, J. Seibt, P. Marquetand, V. Engel and F. Würthner, *Chem. – Eur. J.*, 2007, **13**, 436–449; (*d*) N. Giuseppone, J.-L. Schmitt, L. Allouche and J.-M. Lehn, *Angew. Chem., Int. Ed.*, 2008, **47**, 2235–2239; (*e*) I. Yu, A. Acosta-Ramírez and P. Mehrkhodavandi, *J. Am. Chem. Soc.*, 2012, **134**, 12758–12773; (*f*) A. Pérez, D. de Saá, A. Ballesteros, J. L. Serrano, T. Sierra and P. Romero, *Chem. – Eur. J.*, 2013, **19**, 10271–10279; (*g*) T. M. Alam, D. R. Dreyer, C. W. Bielawski and R. S. Ruoff, *J. Phys. Chem. B*, 2013, **117**, 1967–1977.

3 B. M. Schulze, N. T. Shewmon, J. Zhang, D. L. Watkins, J. P. Mudrick, W. Cao, R. Bou Zerdan, A. J. Quartararo, I. Ghiviriga, J. Xue and R. K. Castellano, *J. Mater. Chem. A*, 2014, **2**, 1541–1549.

4 (*a*) M. Suárez, J.-M. Lehn, S. C. Zimmerman, A. Skoulios and B. Heinrich, *J. Am. Chem. Soc.*, 1998, **120**, 9526–9532; (*b*) A. Mourran, U. Ziener, M. Möller, M. Suarez and J.-M. Lehn, *Langmuir*, 2006, **22**, 7579–7586.

5 W. J. Mitchell, A. J. Ferguson, M. E. Köse, B. L. Rupert, D. S. Ginley, G. Rumbles, S. E. Shaheen and N. Kopidakis, *Chem. Mater.*, 2008, **21**, 287–297.

6 W. J. Mitchell, N. Kopidakis, G. Rumbles, D. S. Ginley and S. E. Shaheen, *J. Mater. Chem.*, 2005, **15**, 4518–4528.

7 J. T. Edward, *J. Chem. Educ.*, 1970, **47**, 261.

8 H. C. Chen and S. H. Chen, *J. Phys. Chem.*, 1984, **88**, 5118–5121.

9 F. Perrin, *J. Phys. Radium*, 1936, **7**, 1–11.

10 S. Hansen, *J. Chem. Phys.*, 2004, **121**, 9111–9115.

11 (*a*) A. Jerschow and N. Müller, *J. Magn. Reson.*, 1997, **125**, 372–375; (*b*) M. Nilsson and G. A. Morris, *J. Magn. Reson.*, 2005, **177**, 203–211; (*c*) M. A. Connell, P. J. Bowyer, P. Adam Bone, A. L. Davis, A. G. Swanson, M. Nilsson and G. A. Morris, *J. Magn. Reson.*, 2009, **198**, 121–131.

12 S. Dong, B. Zheng, M. Zhang, X. Yan, X. Ding, Y. Yu and F. Huang, *Macromolecules*, 2012, **45**, 9070–9075.

